Eclipse Prediction and Orbit Improvement for Asteroids: Theory and Application to Near Earth Asteroids

P. Tricarico[1,2,*], N. C. Hearn[1], G. Lake[1,3] and G. Worthey[1]
[1]*Department of Physics and Astronomy, Washington State University, Pullman, Washington*
[2]*Planetary Science Institute, Tucson, Arizona*
[3]*Institute for Theoretical Physics, University of Zurich, Zurich, Switzerland*
[*]*Corresponding author. E-mail: tricaric@psi.edu*

ABSTRACT

Asteroids can be eclipsed by other bodies in the Solar System, but no direct observation of an asteroid eclipse has been reported to date. We describe a statistical method to predict an eclipse for an asteroid based on the analysis of the orbital elements covariance matrix. By propagating a set of Virtual Asteroids to an epoch correspondent to a close approach with a Solar System planet or natural satellite, it is possible to estimate the probability of a partial or total eclipse.

The direct observation of an eclipse can provide data useful to improve the asteroid orbit, especially for dim asteroids typically observed only for a few days. We propose two different methods: the first, based on the inclusion of the apparent magnitude residuals into the orbit's least squares minimization process, capable of improving the asteroid's nominal orbit and the related covariance matrix; the second, based on weighting different Virtual Asteroids in relation to their apparent magnitude during the eclipse, useful for recovery purposes.

As an application, we have numerically investigated the possibility of a Near Earth Asteroid eclipsed by the Moon or the Earth in the 1990-2050 period. A total of 74 distinct eclipses have been found, involving 59 asteroids. In particular, the asteroid (99942) Apophis has a probability of about 74% to enter the Moon's penumbra cone and a probability of about 6% to enter the umbra cone on April 14, 2029, less than six hours after a very close approach to Earth.

Subject headings: asteroids, eclipses

1. Introduction

Near Earth Asteroids, or NEAs, have received increased attention by the scientific community and the public at large in recent years. Over the past decade, the rate of discovery for NEAs has increased by an order of magnitude to the current rate of roughly 500 NEAs per year (Chamberlin 2005).

In this paper, we provide a catalog of past and future asteroid eclipses, and propose to use eclipses of asteroids to further constrain their orbits. Here, an eclipse refers to a period when an NEA passes through the shadow of the Earth or the Moon. Simply determining whether an eclipse occurs allows one to accept or reject many possible orbits for an asteroid. Observing the decrease in luminosity due to its travel through the umbra or penumbra cones would add to the precision of its position in the sky. A total eclipse (passage through the umbra cone) would place significant limits on the distance to the asteroid.

Observing the eclipse of an asteroid is not a trivial matter, even if one has good knowledge of the asteroid's position. Eclipses of an asteroid by the Moon's shadow can occur at any lunar phase. Depending on the solar elongation of the asteroid during the eclipse, the change in luminosity may be visible from an entire hemisphere on Earth, or may not be observable anywhere on Earth.

The prediction of such events requires a statistical treatment of the accuracy of the orbital elements. The approach used here involves sampling the most likely set of orbital elements, based on existing observations,

and then simulating the dynamics of objects on these orbits with passing time. We also need a good understanding of the factors contributing to the changes in apparent magnitude during the eclipse.

The plan of the paper is as follows. In Section 2, we introduce the tools needed to describe the eclipse of an asteroid. In Section 3, we apply these tools to the case of NEAs eclipsed by the Earth and the Moon. In Section 4, we estimate the eclipse probability for NEAs. Conclusions follow in Sections 5.

2. Statistical Eclipse Prediction

Our statistical method involves the use of Virtual Asteroids (VAs, see Milani *et al.* (2002)) in conjunction with the concept of an Eclipse Plane (EP) to determine the probability of an eclipse. The theory is very similar to NEAs impact prediction, with eclipse cones playing the role of the target body, and the EP replacing the Target Plane (TP, see Milani *et al.* (2002)).

2.1. Eclipse Geometry

Given a spherical body with a radius r, at a distance D from the Sun, the semi-opening angle for the *penumbra* and the *umbra* cones are, respectively $\alpha_{p,u} = \arcsin((r \pm R)/D)$, with R equal to the Sun's radius, the "$+$" sign for α_p and the "$-$" sign for α_u. The radius $q_{p,u}$ of each section of the cone at a distance d from the center of the spherical body and along the Sun-body line is $q_{p,u} = (r + d\sin(\alpha_{p,u}))/\cos(\alpha_{p,u})$. When $r < R$, as is always the case in the Solar System, $\alpha_p > 0$ and $\alpha_u < 0$, and the umbra cone has a finite length $l = r/\sin(-\alpha_u)$. The Earth's umbra cone length ranges from 3.55 LD to 3.67 LD (LD = Lunar Distance = 384400 km), while for the Moon it is in the range between 0.96 LD and 1.00 LD, depending on the distance between these objects and the Sun. In our computations we assume $R = 6.95 \times 10^5$ km. The cones are aligned on the Sun-body line, keeping into account the light-time delay.

2.2. Virtual Asteroids

In order to predict an eclipse for an asteroid, we need a statistical description of the asteroid's dynamics. This statistical description is necessary because the asteroid's orbital elements are determined only up to some uncertainty. The information on the uncertainty on each orbital element and on the correlation between orbital elements is provided by the covariance matrix, as a result of a least-squares minimization iterative process. The covariance matrix allows the generation of an arbitrary number of Virtual Asteroids, all within the orbital elements uncertainty. The major advantage of sampling the asteroid orbital uncertainty with VAs is that each VA has the same probability to represent the asteroid, and this greatly simplifies a statistical interpretation of the asteroid dynamics related to the eclipse. The VAs provide the statistical description we need. An introduction to VAs and their use can be found in Milani *et al.* (2002).

For the analysis described in Section 3 we generate VAs using *Principal Components Analysis* technique (Jolliffe 1986), also referred to as the Monte Carlo method in the literature. In particular, we will work with the full 6×6 covariance matrix computed at an epoch in the middle of the observational arc of the asteroid.

2.3. The Eclipse Plane

Given the positions of the Sun, the eclipsing body and an asteroid, the EP is defined as the plane containing the asteroid, orthogonal to the Sun-body line (see Fig. 1). As the asteroid's position changes with time, the position of the EP is updated and a new data point is added to the plane. When the asteroid is represented by a cloud of VAs (see Section 2.2), each VA contributes data points to a different EP. Every data point in the plane represents the VA at a different time, and the three possible VA states are represented: outside penumbra, inside penumbra, and inside umbra. When all the different EPs are generated, they're stacked, to obtain the final asteroid's EP.

The eclipse probability can be estimated simply as the fraction of VAs eclipsed, with two different probabilities for penumbra and umbra eclipse. The sensitivity of this probability estimate is clearly limited by the number of VAs used. For the purpose of this work, we are interested in probabilities of the order of 0.01 or greater, achieved by using 512 VAs for each asteroid, in order to limit fluctuations.

2.4. Apparent Magnitude Computations

During the eclipse, the apparent magnitude V of an asteroid is

$$V = H + 5\log_{10}(d \cdot r) + P(\phi, G) + Q(\gamma) \qquad (1)$$

with H the absolute magnitude of the asteroid, d and r the distances of the asteroid from the observer and the

Sun in AU, respectively, $P(\phi, G)$ is a phase relation function, ϕ is the phase angle (Sun-asteroid-observer angle), G is the slope parameter, $Q(\gamma)$ eclipse correction, and γ is the ratio between the eclipsed Sun light flux and the nominal solar light flux. The parameterization used for the phase relation function $P(\phi, G)$ is

$$\begin{aligned} P(\phi, G) &= -2.5 \log_{10}\left((1-G)\Phi_1(\phi) + G\Phi_2(\phi)\right) \\ \Phi_1(\phi) &= \exp\left(-3.33(\tan(\phi/2))^{0.63}\right) \\ \Phi_2(\phi) &= \exp\left(-1.87(\tan(\phi/2))^{1.22}\right) \ . \end{aligned} \quad (2)$$

(Bowell *et al.* 1989; Cox 2000). The value of G adopted for all the asteroids is the default value $G = 0.15$. The eclipse correction $Q(\gamma)$ is a simple function of γ:

$$Q(\gamma) = -2.5 \log_{10}(\gamma) \quad (3)$$

and can be derived considering that, if the light flux from a partially eclipsed solar disk is $\gamma F_\odot$ and the light flux from whole solar disk is $F_\odot$, the apparent magnitude of the Sun, observed from the asteroid is $m_\gamma = -2.5 \log_{10}(\gamma F_\odot / F_0) = m_\odot - 2.5 \log_{10}(\gamma)$, with F_0 the reference light flux for $m = 0$. The parameter γ is in the range between 1 and 0, with the limit values relative to the unobstructed Sun and to a total eclipse, respectively. For the numerical computation of γ we take into account the eclipse geometry and the solar limb darkening. The limb darkening effect (Cox 2000) can be described by

$$\frac{I_\lambda(\psi)}{I_\lambda(0)} = 1 - u_2 - v_2 + u_2 \cos(\psi) + v_2 \cos^2(\psi) \quad (4)$$

with ψ denoting the angle, measured from the Sun's center, between the observer and the point on the Sun's surface. Here, $I_\lambda(\psi)$ is the light intensity observed at wavelength λ. The values of the constants u_2 and v_2 relative to $\lambda = 550$ nm, used in the following computations, are u_2 = 0.93 and v_2 = -0.23 (Cox 2000). The angle θ between the solar disk center and a point on the Sun's surface, as measured from the asteroid, is related to ψ through the transformation

$$\sin(\psi) = \sin(\theta)/\sin(\Omega) \quad (5)$$

valid in the limit of $R \ll D$, where Ω is the solar disk semi-aperture, and $0 \leq \theta \leq \Omega$.

Using Eq. (4) and Eq. (5), it is possible to estimate numerically the fraction γ of light flux reaching the asteroid. In particular, using the normalization $N = 1/(1 - u_2/3 - v_2/2)$ the integral of Eq. (4) over the fraction Γ of the solar disk visible from an asteroid is always between 0 and 1. The variable Γ can be easily computed: with Ω_s and Ω_b being the semi-aperture angles for the solar disk and the eclipsing body disk, respectively, and ζ_{sb} the angle between the two disks centers, all measured from the asteroid, we define β_b and β_s from

$$\cos(\beta_b) = (\Omega_b^2 + \zeta_{sb}^2 - \Omega_s^2)/(2\Omega_b\zeta_{sb}) \quad (6)$$

$$\cos(\beta_s) = (\Omega_s^2 + \zeta_{sb}^2 - \Omega_b^2)/(2\Omega_s\zeta_{sb}) \ . \quad (7)$$

We then let

$$A_b = \Omega_b^2(\beta_b - \sin(\beta_b)\cos(\beta_b)) \quad (8)$$

$$A_s = \Omega_s^2(\beta_s - \sin(\beta_s)\cos(\beta_s)) \quad (9)$$

and the visible fraction Γ of the solar disk, sorted by decreasing value of ζ_{sb}, is

$$\Gamma = \begin{cases} 1 & \Omega_s + \Omega_b \leq \zeta_{sb} \\ 1 - (A_b + A_s)/(\pi\Omega_s^2) & \Delta \leq \zeta_{sb} < \Omega_s + \Omega_b \\ 1 - \Omega_b^2/\Omega_s^2 & \zeta_{sb} < \Delta, \Omega_b < \Omega_s \\ 0 & \zeta_{sb} < \Delta, \Omega_s \leq \Omega_b \end{cases} \quad (10)$$

with $\Delta = |\Omega_s - \Omega_b|$. These four cases are relative to the body disk outside, crossing and inside the solar disk, with the last case separated into two sub-cases, based on the relation between Ω_s and Ω_b. In general, the difference between γ and Γ depends on the position of the body with respect to the solar disk.

By using this formalism we can compute the maximum apparent magnitude effect due to an eclipse for a generic asteroid, as a function of the close approach distance from Earth or Moon, keeping into account the Earth to Sun and Moon to Sun distance range. The result is reported in Fig. 2, where the maximum effect is obtained by forcing the perfect Sun-body-asteroid alignment, so that the body is obscuring the brighter part of the solar disk.

Two important classes of error have to be considered when trying to predict an asteroid magnitude: the light curve of the asteroid, and the atmosphere, oblateness and surface features of the eclipsing body. An accurate light curve is required in order to correctly interpret the observations. The light curve amplitude of the asteroid can be bigger than the eclipse effect, and should be measured immediately before and after the eclipse, in order to account for possible changes in the rotation due to the close approach to the eclipsing body, and also to account for complex light-curves related to tumbling asteroids (Pravec *et al.* 2005).

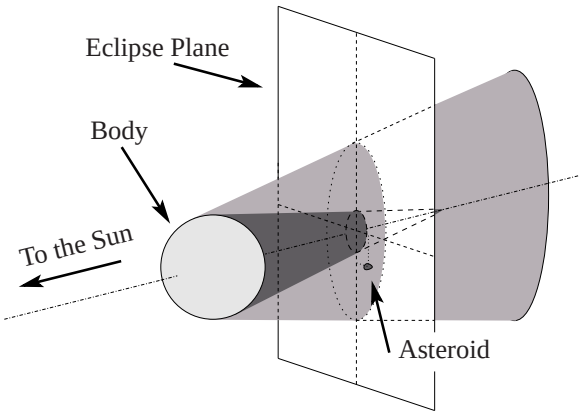

Fig. 1.— Eclipse Plane. The light is coming from the Sun on the left side of the diagram, and the penumbra and umbra cones are visible. At any time, the eclipse plane is orthogonal to the Sun-body line, and contains the asteroid.

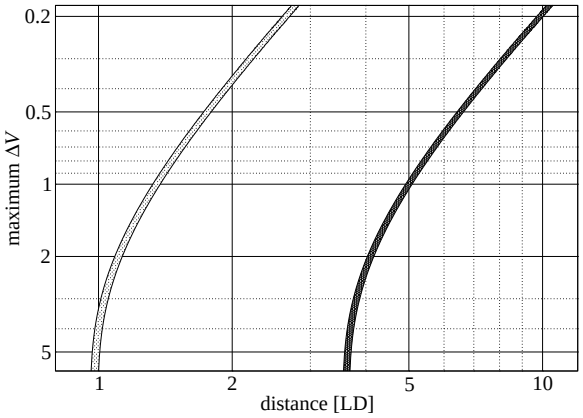

Fig. 2.— Maximum apparent magnitude effect due to an eclipse, as a function of the distance between the asteroid and the Moon (left band, light gray) or the Earth (right band, dark gray). The width of each band is related to the range of the distance D between the eclipsing body and the Sun.

When the eclipsing body has an atmosphere, as is the case for NEAs eclipsed by the Earth, the apparent magnitude V can differ from that estimated here because of refraction and scattering of sunlight through the atmosphere. These effects become more and more important as a smaller fraction of the solar disk is illuminating the asteroid. In particular, the asteroid's apparent magnitude V will have a finite value even during the total eclipse phase. An estimate of this effect can be obtained from the Moon's apparent magnitude during a total Moon eclipse: according to Mallama (1993), the apparent magnitude of the Moon fades from -12.7 outside the eclipse to +1.4 when the Moon reaches the maximum eclipse point. This gives an estimate of the maximum effect of the eclipse, $\Delta V_{\max} = 14.1$, for an object at the distance of 1 LD from the Earth. This limit can be bigger by up to 5 magnitudes after volcanic eruptions (Mallama 1993). The maximum eclipse effect at distances different from 1 LD can be obtained using inverse-square-law scaling. Body oblateness and a non-smooth body surface can also represent sources of error to the magnitude estimate, the former mainly during the penumbra eclipse, the latter mainly at the umbra-penumbra interface.

2.5. Eclipse Observation and Orbit Improvement

An appreciable fraction of relatively small NEAs are discovered during their close approach to the Earth-Moon system, and can be followed only for a limited number of days. This means that their observed arc is extremely short at the moment of the close approach, and their orbit can be determined with very limited accuracy. In case of an eclipse during the passage of the asteroid, it is possible in principle to measure the main features of the eclipse: the epoch relative to the beginning and the end of the total eclipse, and the magnitude variations during the partial eclipse phase. These data can help to improve the orbit accuracy: intuitively, if a set of VAs is used to statistically describe the orbital evolution of the asteroid, in general every VA will enter and leave the umbra region at different times and with a different geometry; the comparison between observations and predictions for different VAs could restrict the space of parameters to a subset having a behavior compatible with the observations. For total eclipses, accurate measurements of the umbra entering and leaving times are indirect observer-asteroid distance measurements: the intersection between a 2D surface (the umbra cone)

and the line of sight from the observer to the asteroid provides the asteroid position within the measurement and model errors.

We propose two different methods to improve the asteroid orbit: one based on least squares minimization of a modified minimized function, and another based on VAs weighting.

The standard function minimized using least squares techniques is the sum over all the astrometric observations of the residuals δ on right ascension and declination

$$f = \sum_{\rm obs} \left(\left(\frac{\delta_{\rm RA}}{\sigma_{\rm RA}} \right)^2 + \left(\frac{\delta_{\rm DEC}}{\sigma_{\rm DEC}} \right)^2 \right) \qquad (11)$$

with an estimated accuracy σ of the order of 1.0 arcseconds for observations by modern telescopes using CCD cameras. This function can be extended, to include the eclipse magnitude observations

$$f' = f + \sum_{\rm obs} \left(\frac{\delta_{\rm mag}}{\sigma_{\rm mag}} \right)^2 \qquad (12)$$

with $\delta_{\rm mag}$ the magnitude residual and $\sigma_{\rm mag}$ the estimate of the total error on the magnitude measurement. A major problem related to this method is the correct estimate of $\sigma_{\rm mag}$, taking into account the asteroid light curve and effect of the eclipsing body's atmosphere, oblateness and surface features. We are still investigating the applicability of this method; a direct asteroid eclipse observation would provide a great opportunity to test and validate this method.

An alternative approach is the following: we select a subset of all the VAs by assigning to each VA a weight w defined as

$$w^2 = \frac{1}{N_{\rm obs}} \sum_{\rm obs} \left(\frac{\delta_{\rm mag}}{\sigma_{\rm mag}} \right)^2 \qquad (13)$$

and selecting all the VAs below a threshold $w_{\rm max}$. In this case $\delta_{\rm mag}$ represents the magnitude residual for the VA considered. This method doesn't improve the nominal solution, but can be useful to determine the possible sky projection of the selected VAs after an observed eclipse, for recovery purposes. As an example, see Section 3.2 and Fig. 6 for the case of 2004 ST_{26}.

3. NEAs Eclipsed by Earth and Moon

As an application of this eclipse prediction method, we investigate the possibility for each known NEA to be eclipsed by the Earth or the Moon. We have propagated numerically the orbit of all the known NEAs, 3444 asteroids, in the period 1990-2050, using the orbits and covariance matrices computed by the NEODyS group (Chesley & Milani 2000) that were available on August 17, 2005. The dynamical system includes the Sun, all planets, and the Moon, plus the massless VAs. The numerical integration is performed using the ORSA[1] framework. In particular, a modified version of the 15th order RADAU integrator (Everhart 1985) has been used, with a nominal accuracy of 10^{-12}. The difference between the original algorithm and the modified version is that this modified version doesn't integrate the Solar System objects, as their positions and velocities are read at each internal timestep from the JPL ephemeris DE405 to ensure the maximum possible accuracy, while the VAs are numerically propagated. The accuracy of this modified RADAU integrator, as implemented in the ORSA framework, has been extensively tested during the development of ORSA. In particular, the minimum Earth/asteroid distance is always in very good agreement (i.e. well within the orbital elements uncertainties) with the data provided by the NEODyS website (Chesley & Milani 2000).

The results of this analysis have been collected in Table 1. In particular, we have recorded all the eclipses with a penumbra eclipse probability $P_p \geq 0.01$ and a fraction of solar disk visible $\Gamma \leq 0.99$, that is, all the eclipses within 10 LD if by the Moon, and within 40 LD if by the Earth. A total of 74 distinct eclipses have been found, involving 59 asteroids. Of the 74 eclipses found, 58 are by Earth and 16 by the Moon. A detailed analysis of the probability of an asteroid eclipse and an estimate of the expected number of eclipses per year are provided in Section 4.

We have found three classes of *special* asteroid eclipses: *double eclipses*, *multiple eclipses*, and *immediate eclipses*. These classes are not mutually exclusive, and we have examples of eclipses belonging to more than one class. An asteroid experiences a *double eclipse* if it is eclipsed by both Earth and Moon during the same close approach; more details are provided in Section 3.5. A different pattern is observed in 3 other cases, when the same asteroid experiences several eclipses during different close approaches. We will refer to these events as *multiple eclipses* (see Section 3.6). Another class is represented by asteroids

[1] `http://orsa.sourceforge.net`

with an eclipse happening during the same close approach as the discovery; we will refer to these events as *immediate eclipses*, and the asteroids with eclipses belonging to this class are listed in Table 2 and studied in more detail in Section 3.7.

In the following sections we describe some particular cases found, beginning with the extremely unusual case of (99942) Apophis.

3.1. (99942) Apophis

The asteroid (99942) Apophis was discovered on 2004 June 19 by Roy Tucker, David Tholen, and Fabrizio Bernardi while observing from the Kitt Peak National Observatory, Arizona. Announced by Gilmore *et al.* (2004), this asteroid has set the highest level of attention since the introduction of the *Torino Scale* (TS, Morrison *et al.* 2004), reaching the TS-4 level. Pre-discovery observations of (99942) Apophis excluded the possibility of an impact with the Earth on 2029 April 13, but still leaving the possibility of an impact at successive epochs. Radar observations in January 2005 (Benner *et al.* 2005) and September 2005 (Giorgini *et al.* 2005) further improved the orbit of the asteroid. In particular, for our computations we are using the orbit solution computed including all the radar observations mentioned above.

Less than one day after the close approach to Earth on 2029 April 13, this asteroid has a chance of being eclipsed by the Moon. The passage of the VAs close to or inside the Moon's shadow is visible in Fig. 3. The VAs cross the Moon's shadow cones at a distance between 0.70 and 0.75 LD from the Moon, where the penumbra disc radius ranges between 2981 and 3081 km (increasing with distance), and the umbra disc between 395 and 495 km (decreasing with distance). About 74% of all the VAs enter the penumbra, starting as early as 2029 Apr 14 at 2:41 TDT (TDT is the Terrestrial Dynamical Time timescale) and leaving it no later than 3:41 TDT of the same day, lasting up to 42 minutes, 32 minutes on average. A smaller fraction, about 6% of all the VAs, enter the umbra starting as early as 3:06 TDT and leave it no later than 3:14 TDT, lasting up to about 6 minutes, with an average of 4 minutes. The VA relative to the nominal orbit enters the penumbra at 3:12 TDT and leaves it at 3:40 TDT without entering the umbra (see Fig. 3). This eclipse will not be visible from Earth because the solar elongation of this asteroid will range between about 15.9° and 17.7° during the eclipse. A diagram showing the expected magnitude curve for (99942) Apophis is shown in Fig. 4. Simulated magnitudes are shown for observations both from Earth (or from a low orbit satellite) and from the Moon (in case a telescope will be in place on the side of the Moon facing the Earth by 2029).

3.2. 2004 ST_{26}

This asteroid has a 18% probability that it crossed the lunar penumbra on 2004 September 22 at 2:08 TDT, and about 4% probability of having crossed the umbra cone. The eclipse plane is provided by Fig. 5.

This case can be used to show the ideas behind the orbit improvement connected with the direct observation of an asteroid eclipse, as described in Section 2.5. In Fig. 6 we have the distribution of apparent magnitude, as a function of the distance from Earth, for all the generated VAs at a fixed time. Each data point represents a different VA. An eclipse observation at this time could select, within the magnitude measurement errors, the fraction of VAs compatible with observations: As an example, an apparent magnitude measurement of $V = 19.0 \pm 1.0$ would indicate a distance from Earth of about 0.00278 AU, promoting VAs (and relative orbits) at that distance. Additional information on the apparent magnitude curve, obtained with successive measurements, could further improve the relative weight of different asteroids to help in the selection of the most probable region in the space of the orbital elements.

3.3. 2003 WT_{153}

The asteroid 2003 WT_{153} experiences one of the 15 eclipses found with penumbra eclipse probability $P_p = 1.00$ (see Table 1), that is, all the VAs relative to this asteroid crossed the Earth's penumbra cone on 2003 Nov 28 at 8:44 TDT. This eclipse, not directly observed, lasted about 130 minutes, with an important effect on the apparent magnitude (see Fig. 7).

3.4. 2003 SY_4

This asteroid is the only one found, a posteriori, with astrometry measurements during an eclipse. In particular, part of the discovery observations were made during the eclipse listed on Table 1. Discovered by M. Block at the LPL/Spacewatch II observatory (Tichy *et al.* 2003) on 2003 September 17 with a series of six observations, it turns out that the first two observations, at 6:58 TDT and 7:19 TDT, were inside

the eclipse window. The asteroid 2003 SY_4 has been eclipsed by the Earth on 2003 September 17 between 6:48 TDT and 7:24 TDT, and it crossed, with a probability of 100%, the penumbra cone. Since the minimum solar disk fraction visible during the eclipse is 0.98, the effect of the eclipse is much smaller than the magnitude measurements error: the measured apparent magnitude during the eclipse is $V_{\rm obs} = 17.9$ while the computed one is $V_{\rm comp} = 17.7$ (neglecting all the error sources described in Section 2.4).

3.5. Double Eclipses

We have found 9 different double eclipses, i.e., eclipses when the same asteroid is eclipsed by both Earth and the Moon during the same close approach, usually within the span of a few hours. The 9 events found in our numerical simulations are: 2004 TB_{10} in 1990, 2003 SW_{130} in 1990, 1998 BT_{13} in 1998, 2001 FE_{90} in 2009, 2004 BL_{86} in 2015, 2001 GP_2 in 2020, 2004 UT_1 in 2022, 1999 VX_{25} in 2040, 2005 KA in 2042.

The case of 1998 BT_{13} is the only one with probability 1.00 for both penumbra eclipses. The case of 2004 UT_1 is also interesting because the two eclipses can be *connected*, i.e. the asteroid can be eclipsed by Earth and Moon at the same time, because the second eclipse by the Earth can start before the first eclipse, by the Moon, is finished.

3.6. Multiple Eclipses

We have *multiple eclipses* when the same asteroid experiences several eclipses during different close approaches. We have found 3 such cases: 2001 LB (2012, 2023), 2003 WT_{153} (2003, 2030), 2003 YT_{70} (1999, 2001, 2005, 2007, 2009). In particular, all the multiple eclipses found involve the Earth. The multiple eclipses pattern for the asteroid 2003 YT_{70} is related to its orbital period being very close to 2 years.

3.7. Immediate Eclipses

We have *immediate eclipses* every time an asteroid experiences an eclipse during the same close approach as its discovery. We have collected all 18 eclipses belonging to this class in Table 2. In particular, 11 immediate eclipses are by the Earth and 7 by the Moon. We have investigated the relation between the absolute magnitude H of the asteroid involved and the delay $\Delta t = t_e - t_d$ between eclipse time t_e and asteroid discovery time t_d. As Fig. 8 suggests, we can distinguish between immediate eclipses by bright asteroids ($H \lesssim 26$) or by dim asteroids ($H \gtrsim 26$). The 8 eclipses of bright asteroids (upper half of Fig. 8, all by Earth) exhibit delays of several days, with a tendency toward eclipse after discovery, while the 10 eclipses of dim asteroids (lower half of Fig. 8, 3 by Earth, 7 by Moon) have much shorter delays, with a strong tendency toward eclipse before discovery.

To try to explain this behavior we must consider that dim asteroids, with an estimated diameter typically between 10 and 30 meters, can be observed by many active telescopes only for a limited amount of time (often only 2 or 3 nights), and for this reason dim asteroids can be discovered only when the observer/asteroid distance is close to the minimum. Also, even if potentially visible, a dim asteroid can remain undetected for several nights because of many factors related to the observatory hardware, asteroid dynamics, and other selection effects (see Jedicke *et al.* (2002) for a review). Now, if we consider that an eclipse by Earth or the Moon can take place only at a time close to the middle of the discovery time window, and that this discovery window is small for dim asteroids and relatively large for bright ones, it is easy to realize that we have only 1 or 2 nights to discover a dim asteroid before the eclipse, while we have several nights to discover a bright asteroid before the eclipse. Since 2 nights can often be insufficient to discover a dim asteroid, the eclipse is likely to happen before the dim asteroid is discovered. This effect poses substantial limits to the numerical prediction and the direct observation of immediate eclipses involving dim asteroids.

4. Eclipse Probability for NEAs

We attempt now to estimate the probability of two different events: the average eclipse probability per NEA, and the probability for an eclipse to occur at an epoch very close to the discovery epoch of the asteroid.

The average eclipse probability per NEA can be obtained by properly scaling the impact probability between a NEA and the Earth, that Stuart & Binzel (2004) estimate as 1.50×10^{-9} per year per NEA. The scaling factor is the ratio between the eclipse cone longitudinal section and the gravitational capture radius disk of the Earth. This section is well approximated by a trapezoid for the penumbra cone, and by a triangle for the umbra cone. By using the relations developed in Section 2.1, and using the Earth's

gravitational capture radius equal to 7540 km (Stuart & Binzel 2004) when dealing with impact probabilities and the Earth's equatorial radius of 6378 km for geometric computations, and limiting the penumbra cone length to 10 LD for the Moon and to 40 LD for the Earth (that is, about ten times the respective umbra cone length), with a simple algebra we find that the penumbra and umbra scaling factors for the Earth are, respectively, $\sigma_{p,E} \simeq 7300$ and $\sigma_{u,E} \simeq 50$, while for the Moon we get $\sigma_{p,M} \simeq 460$ and $\sigma_{u,M} \simeq 4$. The average eclipse probabilities are $P_{p,E} \simeq 1.1 \times 10^{-5}$, $P_{u,E} \simeq 7.5 \times 10^{-8}$, $P_{p,M} \simeq 6.9 \times 10^{-7}$, $P_{u,M} \simeq 6.0 \times 10^{-9}$, all per year per NEA.

We can scale these probabilities to the number of NEA (3444 asteroids) examined in our analysis, and to the 60 years period monitored, obtaining the expected number of events $N_{p,E} \simeq 2.26$, $N_{u,E} \simeq 0.015$, $N_{p,M} \simeq 0.14$ and $N_{u,M} \simeq 0.0012$. These probabilities can be compared directly to the probabilities of the eclipses found (see Table 1), considering the eclipse probability as a *fractional event*. The sum S of all the probabilities relative to asteroids with eclipses at epochs far from the discovery epoch, i.e. considering only the asteroids that are in Table 1 but not in Table 2, gives $S_{p,E} = 3.40$, $S_{u,E} = 0.02$, $S_{p,M} = 0.93$ and $S_{u,M} = 0.06$. The agreement between estimated and numerically detected number of events for eclipses by the Earth can be considered satisfactory, considering the relatively small number of eclipses found. On the other hand, the sums $S_{p,M}$ and $S_{u,M}$ for eclipses by the Moon are significantly different from the estimates $N_{p,M}$ and $N_{u,M}$, with (99942) Apophis as the major contributor. We notice that, neglecting the contribution from (99942) Apophis, we would have $S_{p,M} = 0.19$ and $S_{u,M} = 0.00$, in satisfactory agreement with the predicted probability. To partially justify this solution to the discrepancy we notice that (99942) Apophis's orbit has been determined with an accuracy that is orders of magnitude better than the average accuracy of all the other asteroids experiencing an eclipse, putting this asteroid somewhat out of statistics. An alternative explanation, still under investigation, is of dynamical nature: the Moon's penumbra and umbra cones can intersect a number of NEAs orbits larger than expected because the Moon, while orbiting around the Earth, is allowed in general to get a bit closer to an asteroid, especially when compared to an hypothetic Moon fixed on the Earth's orbit.

What is the probability for a newly discovered NEA to experience an eclipse during the same close approach of the discovery? We can estimate it using the NEA discovery statistics (Chamberlin 2005). Our analysis extends from 1990 to 2050, but for this section we are limited to the period between 1990 and today. The NEAs discovered between Jan 1, 1990 and August 1, 2005 are $3434 - 134 = 3300$, and in this period only 17 asteroids have experienced eclipses at a time very close to the discovery time (for a total of 18 eclipses, because 1998 BT_{13} experiences a double eclipse). This leads to a probability of about one in 194 for a newly discovered NEA to experience an eclipse at a time very close to the discovery time. If we limit ourselves to the period between Jan 1, 1998 and August 1, 2005 only $3434 - 445 = 2989$ NEAs have been discovered in this period, and only 16 of the original 17 asteroids fall into this period. The probability estimate for this restricted period is of about one in 187. With 439 NEAs discovered in 2003 and 532 discovered in 2004 (Chamberlin 2005), a number of events between two and three per year can be expected, and possibly more, as the six events in 2003.

5. Conclusions

Near Earth Asteroids can be eclipsed by Earth and the Moon as has happened in the past 15 years, and will occur again in the future to known asteroids and to asteroids not yet discovered. We have compiled a catalog, based on numerical simulations, of all the asteroid eclipses between a NEA and Earth or the Moon, in the period 1990-2050, including a total of 74 distinct eclipses involving 59 asteroids. A closer inspection at these eclipses allowed us to determine three different recurring patterns: *double eclipses*, *multiple eclipses*, and *immediate eclipses*. In particular, the analysis of *immediate eclipses* allowed us to explain their apparent tendency to happen within one or two days before the asteroid discovery.

An analysis of the NEAs eclipse probability offers two main results: $i)$ asteroid impact probabilities for Earth and the Moon can be scaled in order to predict asteroid eclipse probability, with satisfactory agreement between predicted and numerically detected number of events; $ii)$ every newly discovered NEA has a probability of about one in 190 to experience an eclipse during the same close approach of the discovery. Given the present rate of discovery, several new eclipses are expected every year involving newly discovered asteroids. With the beginning of a new class of NEOs surveys, such as LSST

(Stubbs *et al.* 2004) and Pan-STARRS (Kaiser & Pan-STARRS Team 2005), it will be possible to cover the entire visible sky to the 24th magnitude in less than a week, enabling discovery rates almost two orders of magnitude greater than all existing surveys combined, hence allowing the direct observation of up to a few hundred NEA eclipses per year. We plan to routinely monitor numerically all NEAs for potential eclipses, using the *Distributed Computing System for Near Earth Objects Hazard Monitoring* (Tricarico 2004) now under construction.

The direct observation of an asteroid eclipse can provide data useful to improve the orbit of the asteroid. We suggest two different methods to improve the asteroid orbit, the first as an extension of the standard least squares method, and the second as a weighting rule for different VAs relative to the asteroid. We plan to test and extend these methods as soon as data relative to direct observations of NEA eclipses will be available.

The theoretical tools developed in this work in order to statistically predict an asteroid eclipse apply to any case of an asteroid eclipsed by a larger spherical body.

We gratefully acknowledge Don Davis, Beatrice Mueller, Steve Kortenkamp and Stu Weidenschilling for their suggestions, comments, and constructive criticisms.

REFERENCES

Benner, L. A. M., Nolan, M. C., Giorgini, J. D., Chesley, S. R., Ostro, S. J., International Astronomical Union Circular, 8477 (2005).

Bowell, E., Hapke, B., Domingue, D., Lumme, K., Peltoniemi, J., Harris, A. W., *Application of photometric models to asteroids*, in *Asteroids II*, Proceedings of the Conference, Tucson, AZ, p. 524-556 (1989).

Chamberlin, A. B., http://neo.jpl.nasa.gov/stats/, (2005).

Chesley, S. R. and Milani, A., *An Automatic Earth-Asteroid Collision Monitoring System*, BAAS, Vol. 32, p. 862 (2000).

Cox, A. N., *Allen's Astrophysical Quantities*, Springer-Verlag, NY (2000).

Everhart, E., *An efficient integrator that uses Gauss-Radau spacings*, in *Dynamics of Comets: Their Origin and Evolution*, Proceedings of IAU Colloq. 83, edited by A. Carusi, G. B. Valsecchi. Dordrecht: Reidel, Astrophysics and Space Science Library, Volume 115, 185-202 (1985).

Gilmore, A. C., Kilmartin, P. M., Young, J., McGaha, J. E., Garradd, G. J., Beshore, E. C., Casey, C. M., Christensen, E. J., Hill, R. E., Larson, S. M., McNaught, R. H., Smalley, K. E., Minor Planet Electronic Circulars, Y-25 (2004).

Giorgini, J. D., Benner, L. A. M., Ostro, S. J., Nolan, M. C., Busch, M. W., International Astronomical Union Circular, 8593, 1 (2005).

Jedicke, R., Larsen, J., Spahr, T., *Observational Selection Effects in Asteroid Surveys and Estimates of Asteroid Population Sizes*, in *Asteroids III*, University of Arizona Press, Tucson, AZ, p. 71-87 (2002).

Jolliffe, I. T., *Principal Component Analysis*, New York: Springer-Verlag (1986).

Kaiser, N., Pan-STARRS Team, *The Pan-STARRS Large Survey Telescope Project*, AAS Meeting Abstracts, 206, (2005).

Mallama, A., *Two Celestial Visibility Projects: 1) The Brightness of an Eclipsed Moon and 2) The Phase Anomaly of Venus*, BAAS, Vol. 25, p. 1334 (1993).

Milani, A., Chesley, S. R., Chodas, P. W., Valsecchi, G. B., *Asteroid Close Approaches: Analysis and Potential Impact Detection*, in *Asteroids III*, University of Arizona Press, Tucson, AZ, p. 55-69 (2002).

Morrison, D., Chapman, C. R., Steel, D., Binzel R. P., *Impacts and the Public: Communicating the Nature of the Impact Hazard*, in *Mitigation of Hazardous Comets and Asteroids*, edited by Belton, M. J. S., Morgan, T. H., Samarasinha, N. H, and Yeomans, D. K., Cambridge University Press (2004).

Pravec, P., Harris, A. W., Scheirich, P., Kušnirák, P., Šarounová, L., Hergenrother, C. W., Mottola, S., Hicks, M. D., Masi, G., Krugly, Y. N., Shevchenko, V. G., Nolan, M. C., Howell, E. S., Kaasalainen, M., Galád, A., Brown, P., Degraff, D. R., Lambert, J. V., Cooney, W. R., Foglia, S. *Tumbling asteroids*, Icarus, 173, p. 108-131 (2005).

Stuart, J. S. and Binzel, R. P., *Bias-corrected population, size distribution, and impact hazard for the near-Earth objects*, Icarus, Vol. 170, p. 295-311 (2004).

Stubbs, C. W., Sweeney, D., Tyson, J. A., & LSST, *An Overview of the Large Synoptic Survey Telescope (LSST) System*, AAS Meeting Abstracts, 205 (2004).

Tichy, M., Block, M., Garradd, G. J., McNaught, R. H., Sanchez, S., Stoss, R. Nomen, J., Birtwhistle, P., Smalley, E., Minor Planet Electronic Circulars, S-12 (2003).

Tricarico, P., *A Distributed Computing System for Near Earth Objects Hazard Monitoring*, BAAS, Vol. 36, p. 1141 (2004).

This 2-column preprint was prepared with the AAS LaTeX macros v5.2.

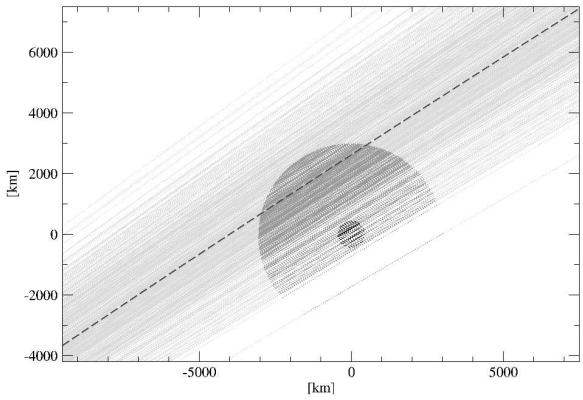

Fig. 3.— Eclipse Plane for (99942) Apophis, eclipsed by the Moon on 2029 Apr 14 around 3:10 TDT. The dark gray circular area represents the penumbra region, while the black circular spot is the umbra region. The x axis is parallel to the Ecliptic plane. The light gray cloud of VAs is moving from bottom left to top right, and is slightly expanding because it just experienced the close encounter with the Earth. The nominal orbit, represented by the dashed line, enters the penumbra region only. About 74% of all the VAs enter the penumbra region, and 6% of all the VAs enter the umbra region.

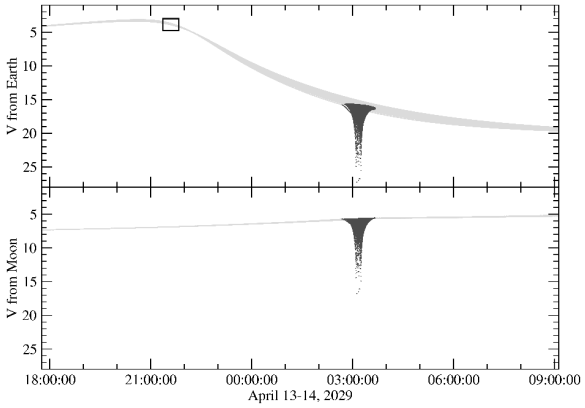

Fig. 4.— Magnitude curve for (99942) Apophis. The upper half of the figure represents the apparent magnitude V of the asteroid as observed from Earth, while the lower half represents the apparent magnitude V as observed from the Moon. The peaks around time 3:10 are the effect of the eclipse. The small box near the top left corner of the plot represents the point of closest approach to Earth; its offset with respect to the brightness maximum is due to the effect of the phase angle $P(\phi, G)$ in the magnitude formula, see Eq. (1). The brightness peak is located about one hour earlier than the close approach time.

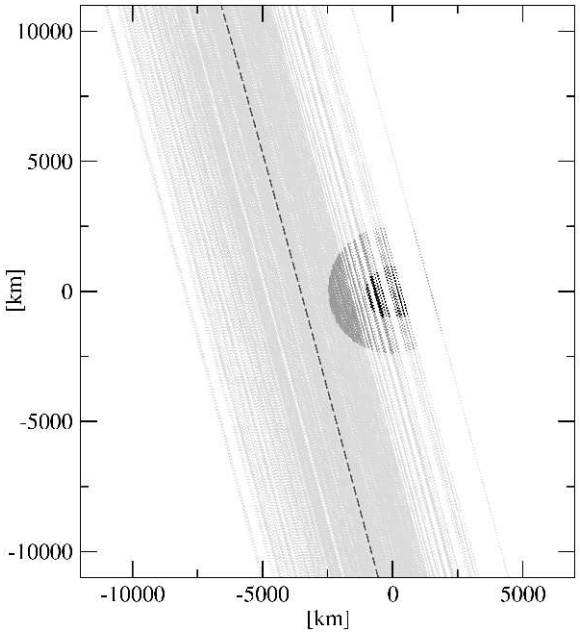

Fig. 5.— Eclipse plane for 2004 ST_{26}, eclipsed by the Moon on 2004 September 22 around 2:08 TDT. About 18% of all the VAs enter the penumbra region, and 4% of all the VAs enter the umbra region. In this case, the VA relative to the nominal orbit, represented by the dashed line, never crosses the penumbra region.

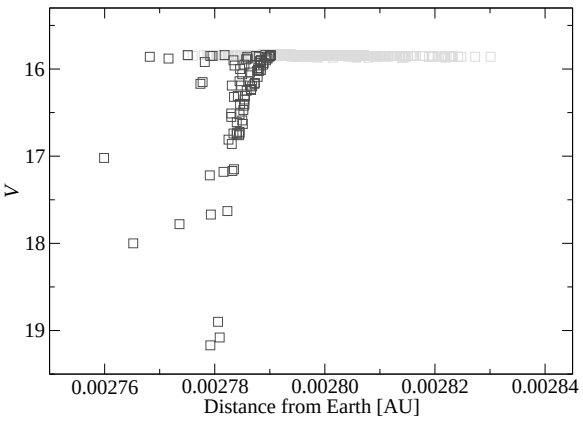

Fig. 6.— Estimated magnitude distribution for all the VAs relative to 2004 ST_{26}, as a function of the distance from Earth, at 2:08 TDT on September 22, 2004. Light gray and dark gray symbols are relative to VAs outside and inside the penumbra cone, respectively.

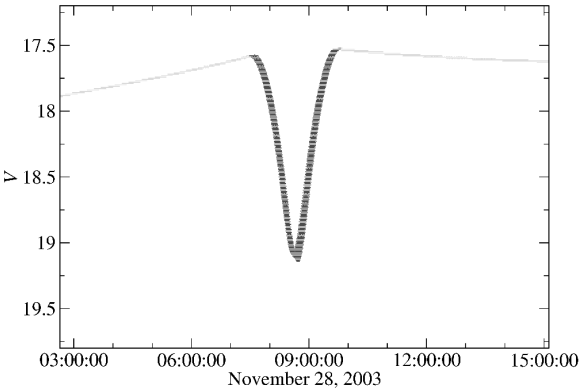

Fig. 7.— Magnitude curve for 2003 WT_{153}, eclipsed by the Earth on 2003 Nov 28 at 8:44 TDT. All the VAs relative to this asteroid crossed the Earth's penumbra cone.

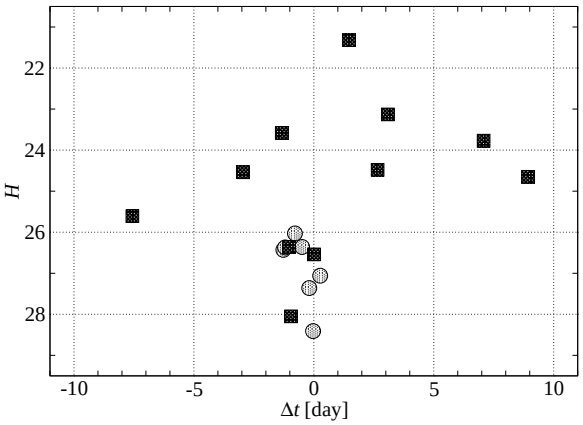

Fig. 8.— Immediate eclipses: asteroid absolute magnitude H versus delay Δt (see text). The square symbol represents eclipses by the Earth, while the circle represents eclipses by the Moon.

TABLE 1

ASTEROIDS ECLIPSED BY EARTH AND MOON.

			penumbra				*umbra*						
asteroid	body	epoch [TDT]	P_p	$\langle T_p \rangle$ [s]	max(T_p) [s]	min(Γ)	P_u	$\langle T_u \rangle$ [s]	max(T_u) [s]	d_E [LD]	λ [$^\circ$]	H	diameter [m]
2004 TB_{10}	Earth	1990 Apr 2.851	0.01	1900	2500	0.40	0.00	–	–	4.7	179.7	21.25	160 – 370
2004 TB_{10}	Moon	1990 Apr 2.985	0.01	1200	1400	0.95	0.00	–	–	4.7	168.0	21.25	160 – 370
2003 SW_{130}	Earth	1990 Sep 20.531	0.06	4600	5900	0.00	0.01	300	400	3.1	179.6	29.12	1 – 10
2003 SW_{130}	Moon	1990 Sep 20.870	0.05	4800	6100	0.95	0.00	–	–	3.7	174.0	29.12	1 – 10
2000 CK_{59}	Earth	1991 Feb 8.776	0.01	18200	20000	0.95	0.00	–	–	17.0	179.8	23.97	40 – 100
1991 TU	Moon	1991 Oct 7.279	0.31	2400	2700	0.92	0.00	–	–	2.5	176.2	28.41	1 – 10
2003 BM_4	Earth	1995 Jul 29.158	0.01	15400	20400	0.99	0.00	–	–	33.0	179.8	24.68	20 – 60
1998 BT_{13}	Earth	1998 Jan 23.374	1.00	3500	3600	0.93	0.00	–	–	6.9	179.6	26.36	20
1998 BT_{13}	Moon	1998 Jan 23.915	1.00	3900	4000	0.98	0.00	–	–	7.2	173.2	26.36	20
1998 DX_{11}	Moon	1998 Feb 23.615	1.00	2800	3000	0.98	0.00	–	–	5.5	173.0	27.06	10 – 20
1999 HC_1	Earth	1999 Apr 18.970	1.00	6900	7400	0.79	0.00	–	–	8.7	179.7	24.48	30 – 80
1999 TM_{13}	Earth	1999 Oct 3.950	1.00	31000	31100	0.98	0.00	–	–	31.0	179.8	23.58	30 – 70
2003 YT_{70}	Earth	1999 Dec 6.974	0.01	42000	50700	0.97	0.00	–	–	21.8	179.8	25.55	20 – 40
2001 UC_5	Earth	2001 Oct 21.724	1.00	4400	4600	0.98	0.00	–	–	24.2	179.8	21.32	160 – 370
2003 YT_{70}	Earth	2001 Dec 6.699	0.03	39600	50100	0.97	0.00	–	–	22.2	179.8	25.55	20 – 40
2002 DQ_3	Earth	2002 Mar 1.482	1.00	29400	29500	0.97	0.00	–	–	21.6	179.8	23.77	50 – 110
2002 VY_{91}	Moon	2002 Nov 11.440	1.00	4300	4400	0.98	0.00	–	–	7.4	171.8	26.03	10 – 30
2005 ES_{70}	Earth	2003 Mar 14.076	0.02	5600	6600	0.97	0.00	–	–	21.3	179.8	23.56	50 – 120
2003 LW_1	Earth	2003 Jun 6.394	1.00	4900	5000	0.97	0.00	–	–	16.8	179.7	23.13	60 – 150
2003 SY_4	Earth	2003 Sep 17.296	1.00	2100	2100	0.98	0.00	–	–	6.2	179.6	26.54	10 – 30
2003 UR_{25}	Earth	2003 Oct 17.634	0.08	28700	38800	0.98	0.00	–	–	32.3	179.8	25.61	20 – 50
2003 UT_{55}	Moon	2003 Oct 26.746	1.00	2000	2100	0.94	0.00	–	–	3.1	174.8	27.36	10 – 20
2003 WT_{153}	Earth	2003 Nov 28.364	1.00	7800	7800	0.25	0.00	–	–	3.0	179.7	28.05	1 – 10
2003 YH_{111}	Earth	2003 Dec 24.350	1.00	14700	15600	0.98	0.00	–	–	18.2	179.7	24.54	30 – 80
2004 HD	Earth	2004 Apr 25.136	1.00	12200	12200	0.94	0.00	–	–	15.3	179.8	24.65	30 – 70
2004 SR_{26}	Moon	2004 Sep 20.964	1.00	2900	3200	0.95	0.00	–	–	4.3	166.8	26.43	10 – 30
2004 ST_{26}	Moon	2004 Sep 22.089	0.18	800	1200	0.00	0.04	400	500	1.1	117.2	26.37	10 – 30
2001 SE_{270}	Earth	2005 Sep 20.072	0.02	16500	20800	0.99	0.00	–	–	33.8	179.8	25.10	20 – 60
2003 YT_{70}	Earth	2005 Dec 6.364	0.03	41000	51700	0.97	0.00	–	–	22.2	179.8	25.55	20 – 40
2004 YG_1	Earth	2005 Dec 23.741	0.01	5800	8900	0.98	0.00	–	–	26.8	179.7	21.35	140 – 320
2000 TH_1	Earth	2007 Oct 6.537	0.01	13200	17600	0.99	0.00	–	–	36.1	179.8	22.36	90 – 220
2003 YT_{70}	Earth	2007 Dec 6.345	0.01	34500	51700	0.97	0.00	–	–	22.2	179.8	25.55	20 – 40
1998 SD_9	Earth	2008 Sep 9.407	0.02	5900	7000	0.95	0.00	–	–	17.0	179.8	24.15	40 – 100
1998 VF_{32}	Earth	2009 Nov 18.679	0.02	4700	6000	0.97	0.00	–	–	21.0	179.8	21.15	180 – 400
2001 FE_{90}	Earth	2009 Jun 30.402	0.01	4700	5900	0.80	0.00	–	–	8.4	179.8	19.81	330 – 730
2001 FE_{90}	Moon	2009 Jun 30.632	0.02	4200	4800	0.99	0.00	–	–	8.6	173.3	19.81	330 – 730
2003 YT_{70}	Earth	2009 Dec 6.178	0.01	41400	53000	0.97	0.00	–	–	22.9	179.8	25.55	20 – 40
2000 TU_{28}	Earth	2010 Oct 16.730	0.02	12300	13200	0.98	0.00	–	–	30.0	179.8	20.42	190 – 420
2001 LB	Earth	2012 Jun 11.647	0.01	9600	10800	0.98	0.00	–	–	30.6	179.8	20.77	200 – 460
2004 YA_5	Earth	2012 Dec 21.583	0.01	4600	7300	0.99	0.00	–	–	31.2	179.8	22.58	90 – 200
1997 WQ_{23}	Earth	2013 Nov 18.320	0.01	61000	70000	0.99	0.00	–	–	34.1	179.8	20.39	230 – 530
2004 BL_{86}	Earth	2015 Jan 27.205	0.04	1500	1900	0.05	0.00	–	–	3.6	179.6	18.88	500 – 1100

TABLE 1—*Continued*

asteroid	body	epoch [TDT]	*penumbra* P_p	$\langle T_p \rangle$ [s]	max(T_p) [s]	min(Γ)	*umbra* P_u	$\langle T_u \rangle$ [s]	max(T_u) [s]	d_E [LD]	λ [$^\circ$]	H	diameter [m]
2004 BL_{86}	Moon	2015 Jan 27.337	0.03	900	1200	0.93	0.00	–	–	3.7	164.4	18.88	500 – 1100
2002 LY_1	Earth	2016 May 29.100	0.13	14300	18300	0.99	0.00	–	–	38.2	179.8	21.92	120 – 280
2004 SS	Earth	2017 Sep 24.522	0.01	6300	9100	0.92	0.00	–	–	13.5	179.7	21.95	110 – 260
2002 CB_{19}	Earth	2018 Feb 7.188	0.02	6000	8300	0.96	0.00	–	–	17.8	179.8	24.76	30 – 60
1999 LK_1	Earth	2018 May 21.361	0.09	8400	10100	0.96	0.00	–	–	19.8	179.8	22.11	110 – 250
2001 GP_2	Earth	2020 Oct 6.662	0.01	8600	9500	0.00	0.01	4200	5000	1.1	179.3	26.88	10 – 20
2001 GP_2	Moon	2020 Oct 7.075	0.01	3800	3900	0.78	0.00	–	–	1.8	151.0	26.88	10 – 20
2003 AF_{23}	Earth	2021 Jan 7.156	0.03	4800	6100	0.96	0.00	–	–	19.2	179.8	20.58	210 – 480
2004 FH	Earth	2021 Feb 20.918	0.96	3800	9200	0.98	0.00	–	–	25.0	179.7	26.39	20 – 40
2000 PN_8	Earth	2021 Aug 15.655	0.01	8700	11000	0.99	0.00	–	–	35.0	179.8	22.13	100 – 240
1999 FJ_{21}	Earth	2021 Oct 12.873	0.02	7200	9200	0.98	0.00	–	–	27.0	179.8	20.59	220 – 510
23606	Earth	2022 Jul 19.642	1.00	15900	16600	0.99	0.00	–	–	39.8	179.8	18.47	600 – 1300
2004 UT_1	Moon	2022 Oct 25.182	0.05	9800	12300	0.98	0.00	–	–	6.7	179.4	26.43	10 – 30
2004 UT_1	Earth	2022 Oct 25.238	0.06	9400	11300	0.70	0.00	–	–	6.6	179.7	26.43	10 – 30
2001 LB	Earth	2023 Jun 12.402	0.01	10300	10800	0.98	0.00	–	–	30.6	179.8	20.77	200 – 460
2000 YS_{134}	Earth	2023 Dec 29.199	0.15	11100	14800	0.97	0.00	–	–	23.3	179.8	23.24	70 – 160
2005 FG	Earth	2024 Mar 16.098	0.01	17100	28100	0.99	0.00	–	–	33.3	179.8	24.00	50 – 110
99942	Moon	2029 Apr 14.132	0.74	1900	2500	0.00	0.06	250	350	0.35	17.1	19.17	430 – 970
2003 AF_{23}	Earth	2030 Jan 7.410	0.02	4400	6100	0.96	0.00	–	–	19.1	179.8	20.58	210 – 480
2005 CD_{69}	Earth	2030 Feb 25.433	0.01	30300	30800	0.95	0.00	–	–	17.0	179.8	24.11	40 – 90
2003 WT_{153}	Earth	2030 Nov 17.881	0.34	12700	15000	0.91	0.00	–	–	12.9	179.8	28.05	1 – 10
2005 BC	Earth	2034 Jul 15.295	0.01	4000	5200	0.96	0.00	–	–	20.0	179.8	18.12	700 – 1500
2002 AB_2	Earth	2039 Jan 3.978	0.01	10300	12200	0.99	0.00	–	–	35.1	179.8	22.99	60 – 140
2004 ER_{21}	Earth	2039 Mar 18.246	0.04	10900	13500	0.97	0.00	–	–	20.1	179.8	24.29	30 – 80
1999 VX_{25}	Moon	2040 Nov 13.616	0.01	7800	8600	0.98	0.00	–	–	8.0	173.6	26.70	10 – 30
1999 VX_{25}	Earth	2040 Nov 14.063	0.01	11400	12500	0.78	0.00	–	–	7.9	179.7	26.70	10 – 30
2005 KA	Moon	2042 May 4.445	0.01	2900	3300	0.93	0.00	–	–	4.7	178.3	24.73	30 – 70
2005 KA	Earth	2042 May 5.035	0.01	5600	7300	0.40	0.00	–	–	4.7	179.7	24.73	30 – 70
1997 YM_9	Earth	2044 Dec 26.292	0.01	12300	14100	0.93	0.00	–	–	13.5	179.8	24.77	30 – 60
2000 LF_3	Earth	2046 Jun 12.814	0.01	2600	2800	0.27	0.00	–	–	4.3	179.7	21.57	140 – 320
2004 DK_1	Earth	2045 Apr 29.258	0.01	65200	81800	0.99	0.00	–	–	33.3	179.8	21.05	170 – 380
2001 QJ_{142}	Earth	2047 Sep 26.214	0.03	25500	29500	0.99	0.00	–	–	37.3	179.8	23.42	60 – 130

NOTE.—Near Earth Asteroids eclipsed by Earth and Moon in the period 1990-2050, sorted by epoch. Probability P, mean and maximum time T, averaged over the VAs experiencing the eclipse, are reported for penumbra and umbra eclipses. The average Earth distance d_E and Solar elongation λ are also showed. For penumbra eclipses, the minimum Solar Disk Fraction Γ is also provided. The eclipse epoch is referred to the minimum of Γ in case of a partial eclipse, or to the central moment for a total eclipse. Asteroid diameters are obtained from the Near-Earth Asteroids Data Base, European Asteroid Research Node (http://earn.dlr.de/). The absolute magnitude H is obtained from the NEODyS server (Chesley & Milani 2000). This list is limited to eclipses within 40 LD from the Earth and 10 LD from the Moon, with $P_p \geq 0.01$ and min(Γ) ≤ 0.99.

TABLE 2
IMMEDIATE ECLIPSES.

asteroid	object	discovery epoch [TDT]	eclipse epoch [TDT]	Δt [day]
1991 TU	Moon	1991 Oct 7.310	1991 Oct 7.279	-0.031
1998 BT_{13}	Earth	1998 Jan 24.403	1998 Jan 23.374	-1.029
1998 BT_{13}	Moon	1998 Jan 24.403	1998 Jan 23.915	-0.488
1998 DX_{11}	Moon	1998 Feb 23.352	1998 Feb 23.615	0.263
1999 HC_{1}	Earth	1999 Apr 16.311	1999 Apr 18.970	2.659
1999 TM_{13}	Earth	1999 Oct 5.287	1999 Oct 3.950	-1.337
2001 UC_{5}	Earth	2001 Oct 20.251	2001 Oct 21.724	1.473
2002 DQ_{3}	Earth	2002 Feb 22.405	2002 Mar 1.482	7.077
2002 VY_{91}	Moon	2002 Nov 12.227	2002 Nov 11.440	-0.787
2003 LW_{1}	Earth	2003 Jun 3.308	2003 Jun 6.394	3.086
2003 SY_{4}	Earth	2003 Sep 17.291	2003 Sep 17.296	0.005
2003 UR_{25}	Earth	2003 Oct 25.200	2003 Oct 17.634	-7.566
2003 UT_{55}	Moon	2003 Oct 26.938	2003 Oct 26.746	-0.192
2003 WT_{153}	Earth	2003 Nov 29.315	2003 Nov 28.364	-0.951
2003 YH_{111}	Earth	2003 Dec 27.301	2003 Dec 24.350	-2.951
2004 HD	Earth	2004 Apr 16.199	2004 Apr 25.136	8.937
2004 SR_{26}	Moon	2004 Sep 22.234	2004 Sep 20.964	-1.270
2004 ST_{26}	Moon	2004 Sep 23.285	2004 Sep 22.089	-1.196

NOTE.—Near Earth Asteroids experiencing an eclipse during the same close approach relative to their discovery. See Section 3.7 and Figure 8 for more details. The case of 2003 SY_4 is slightly different from all the other eclipses in this table: part of the discovery observations were made during the eclipse, see Section 3.4.